Bridging the gap of storage ring light sources and linac-driven free-electron lasers

S. Di Mitri[1,2*] M. Cornacchia,[2,3] B. Diviacco,[2] G. Perosa,[1,2]
F. Sottocorona[1,2] and S. Spampinati[2]

[1]*Department of Physics, University of Trieste, 34127, Trieste, Italy*
[2]*Elettra-Sincrotrone Trieste S.C.p.A., 34149 Basovizza, Trieste, Italy*
[3]*Stanford Linear Accelerator Center, 2575 Sand Hill Road, Menlo Park, California 94025, USA (retired)*

High-gain free-electron lasers (FELs) are driven by short, high-charge density electron beams as only produced at dedicated single pass or recirculating linear accelerators. We describe new conceptual, technical, and modeling solutions to produce subpicosecond, up to ∼100 µJ-energy extreme ultra-violet and soft x-ray FEL pulses at high- and tunable repetition rates, from diffraction-limited storage ring light source. In contrast to previously proposed schemes, we show that lasing can be simultaneous to the standard multibunch radiation emission from short insertion devices, and that it can be obtained with limited impact on the storage ring infrastructure. By virtue of the high-average power but moderate pulse energy, the storage ring-driven high-gain FEL would open the door to unprecedented accuracy in time-resolved spectroscopic analysis of matter in the linear response regime, in addition to inelastic scattering experiments.

I. INTRODUCTION

Storage ring light sources (SRLS) are advanced tools for the investigation of matter down to the molecular spatial and timescale. However, to cope with their limitation in serving simultaneously high brilliance, coherent diffraction, and timing experiments, several SRLS laboratories are being enlarging their infrastructure with a short wavelength, sub-ps, high-gain free-electron laser (FEL) [1–5]. The construction and operational cost of a multiGeV linac-driven FEL poses the question of whether a high-gain (HG) FEL can be driven by an existing SRLS while not interfering with, and actually complementing the standard multibeamline operation from short insertion devices (IDs).

The search for such hybrid light source dates back to the 1980s [6–14]. Nonetheless, three major showstoppers have so far excluded high-gain lasing from the portfolio of SRLS: (i) 100's A bunch peak current to drive the lasing process, (ii) transparency to the standard multibunch operation, and (iii) modeling of the light source over an arbitrary timescale. The former two subjects have been tackled in the literature with schemes which at best severely limit the number of stored bunches, reduce the average

beam current by orders of magnitude [15–17], or impose intolerable rf impedance and high-momentum compaction to the storage ring [18]. Modeling is basically limited to a differential equation for the beam energy spread [19].

More recently, schemes of coherent harmonic generation (CHG) driven by an external laser have been proposed for the production of sub-ps longitudinally coherent extreme ultra-violet (EUV) pulses at SRLS [20–23], so promising new opportunities for fast science and diffraction imaging. In some of these schemes, state-of-the-art laser technology limits the light pulse repetition rate to ∼1–10 kHz (on top of beam quality disruption after frequent laser-beam interactions), in others, it constrains the wavelength tuning to typically less than ∼10% or so. Because of limited gain in a short undulator, the pulse energy does not exceed the µJ level.

The present study removes the aforementioned showstoppers and pushes forward the capabilities of CHG by demonstrating the feasibility at diffraction-limited SRLS of a high-gain self-amplified spontaneous emission (SASE) [24,25] FEL, characterized by a tunable repetition rate in the range 0.1–100 kHz, tunable photon energy in the range 95–310 eV, and pulse energy up to 100 µJ level over sub-ps pulse durations.

Lasing is simultaneous and transparent to standard multibunch operation of IDs. In particular, the FEL exploits the multiGeV energy and the high-repetition rate of stored bunches, thus expanding the storage ring capability to carry out pump-probe, high-photon flux, and timing experiments on the basis of cost-effective technology and with limited

*simone.dimitri@elettra.eu

impact on the existing infrastructure. The predicted performance result particularly suited for the study of magnetic and electronic structures, as well as sub-ps fine analysis in spectroscopy. This technique is indeed better served by higher repetition rates than provided by normal conducting linacs, but at photon pulse energies 2–4 orders of magnitude lower than those currently available at single-pass x-ray FELs [26].

The concept and the facility footprint are illustrated in Sec. II. Theoretical and numerical results of beam manipulation in the FEL line are presented in Sec. III. Section IV introduces beam envelope tracking for a comprehensive, semianalytical modeling of the SR-HG-FEL. Section V complements it with an analytical insights into beam and FEL properties at equilibrium. Section VI successfully compares the envelope tracking predictions with start-to-end FEL simulations on a single-pass basis. Then, envelope tracking is extended to an arbitrary number of loops to evaluate the equilibrium beam parameters and FEL performance at high-repetition rates. Section VII details technical solutions for the electron beam injection and extraction system, linac technology, and FEL pulse repetition rate. Conclusions are reached in Sec. VIII.

II. CONCEPT AND FACILITY FOOTPRINT

Figure 1 shows the concept of a SRLS upgraded to a SR-HG-FEL. Main ring parameters for our case study are summarized in Table I.

One or several bunches stored in a train are extracted from the SRLS by a fast injection and extraction system, and sent to a dedicated magnetic compressor. This is made of a short linac (rf) run at the zero-crossing phase to impart a linearly correlated energy spread to the beam (energy chirp).
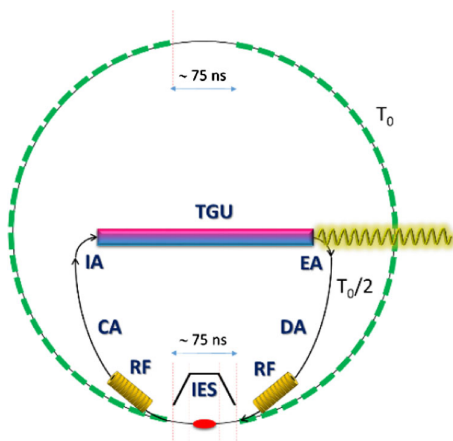
FIG. 1. SRLS upgraded to high-gain FEL. CA = compressive arc, DA = de compressive arc, IA = injection arc, EA = extraction arc, and IES = injection and extraction system. Lasing bunches are in a dark gap of 75 ns.

TABLE I. SRLS parameters for standard ID operation.

Parameter	Value	Units
Circumference length	528	m
Number of achromatic cells	20	
Type of achromatic cell	7-bend	
Length of arc cell	19	m
Average dipole bending angle	44.9	mrad
Revolution period	1.76	μs
Harmonic number	880	
rf bucket spacing	2	ns
Average beam current	<500	mA
Beam mean energy	3	GeV
Damping time (z, x, y)	~9, ~12, ~14	ms
Linear momentum compaction	0.03	%
Bunch duration, rms	9	ps
Peak current	44	A
Relative energy spread, rms	0.08	%
Horizontal emittance	250	pm
Vertical emittance	~1	pm

The linac is followed by a compressive and injection arc (CA, IA) including dipole, quadrupole, and sextupole magnets. Here, the bunch peak current is increased to ~0.7 kA and the rms bunch duration shortened to sub-ps scale via a nonzero momentum compaction. The ~1% relative energy spread accumulated during compression is matched to the narrow FEL energy bandwidth (<0.1%) by a transverse gradient undulator (TGU) traversed by energy-dispersed electrons [27,28].

After lasing, a specular line made of an extraction and decompressive arc (EA, DA) brings the beam back to its initial duration. A second short linac removes the energy chirp, so that the beam is reinjected into the SRLS at equilibrium parameters.

The FEL duty cycle is dictated by the repetition rate of the extraction system, made of fast stripline kickers for on axis swap-out injection [29]. After one loop, bunches are reinjected into an empty series of rf buckets, while keeping the effective ring filling pattern larger than 90%.

As said, after a single loop in the bypass, the beam recovers its original equilibrium state in a damping time or so. If the beam passes through many FEL loops per longitudinal damping time, instead, the emission of synchrotron radiation in the ring is not able to fully wash out the effect of lasing, and a new beam equilibrium state is envisaged due to the persistent FEL perturbation.

The scheme has two strong points. First, the dynamics of lasing bunches is not steady-state, unlike that one invoked in schemes of single bunch FEL [19], microbunched beams [30,31], and low-gain storage ring FELs. This allows one to overcome the Renieri's limit for the maximum average FEL power [32], and up to several W's average power can be generated at 0.1–1 MHz FEL repetition rate, at wavelengths much shorter than those accessible at low-gain storage ring FELs [33].

Second, by keeping bunch compression disentangled from the ring lattice, the scheme can be configured as an upgrade of existing SRLS without modification to the ring lattice, and without affecting the overall ring impedance. This is achieved at the expense of two new arcs and two short linacs, but still with a limited impact on the ring infrastructure, and with affordable costs compared to a brand new, full energy single-pass FEL.

Most of the existing third generation SRLS in the beam energy range $\sim$2–3 GeV feature a natural (geometric) horizontal emittance $\varepsilon_x \sim$ 1–3 nm rad [34]. Many of them are planning or implementing lattice upgrades to multibend cells within the same energy range, which allow the transverse emittances to be lowered by at least one order of magnitude. The charge density is often diluted over tens of ps bunch duration in order to minimize the transverse emittance growth by intrabeam scattering [35].

For our case study, parameters similar to those of the MAX-IV 3 GeV diffraction-limited SRLS are assumed. The lattice is made of 20×7-bend achromatic cells, for a total path length of $C = 528$ m. Drift sections are approximately 5 m long. We assume the same longitudinal charge density than in MAX-IV, but 5 times lower bunch charge ($Q = 1$ nC) over $\sim$4.5 times shorter duration ($\sigma_t = 9$ ps rms); the main rf is 500 MHz. The charge distribution at equilibrium is approximated to a Gaussian. A horizontal equilibrium emittance $\varepsilon_x \approx 250$ pm rad can be realistically expected; it satisfies the diffraction limit condition $4\pi\varepsilon_x \leq \lambda$ [36] at the wavelength of 4 nm with margin. The beam vertical emittance is defined by a transverse coupling coefficient $\varepsilon_y/\varepsilon_x \approx 0.5\%$.

III. ARC COMPRESSOR

A. Magnetic lattice and rf linacs

Scaling of FEL wavelength with electron beam energy and beam emittance suggests that only a relatively high-beam energy (>2 GeV) and a small horizontal emittance (<1 nmrad) would allow efficient lasing at fundamental wavelengths around or shorter than, e.g., $\sim$10 nm. A horizontal geometric emittance at sub-nm level in a SRLS is intrinsically related through synchrotron radiation integrals to a linear momentum compaction as small as $\alpha_c \leq 10^{-4}$, and to a consequently small longitudinal dispersion $R_{56} = \alpha_c C < 0.1$ m over a ring circumference $C \approx 500$ m. Thus, beam manipulation internal to the ring proposed in Ref. [18] is not suited for compression factors larger than 10 or, equivalently, peak currents well above 100 A. We recall that the linear bunch length compression factor is $C = (1 - hR_{56})^{-1}$, with $h = dE/(Edz)$ the z-E linear correlation coefficient in the beam longitudinal phase space, or energy chirp.

Alternatively, a small R_{56} implies that an inconveniently large chirp should be imparted to the beam. The chirp is generated by propagating the beam through a high-accelerating gradient linac:

$$h = \frac{dE}{Edz} = \frac{2\pi}{\lambda_{\rm rf}} \frac{eV\cos\varphi_{\rm rf}}{E_0 + eV\sin\varphi_{\rm rf}} \cong \frac{\sqrt{\sigma_{\delta{\rm cor},0}^2 + \sigma_{\delta,0}^2}}{\sigma_{z,0}}. \quad (1)$$

Here, V is the rf linac peak voltage, $\lambda_{\rm rf}$ is the rf wavelength, $\varphi_{\rm rf}$ ($=0$) is the rf phase (at zero-crossing), $\sigma_{\delta,\rm cor}$, $\sigma_{\delta,0}$, and $\sigma_{z,0}$, the beam energy spread correlated with z, the uncorrelated energy spread, and the bunch length before compression, respectively.

The impasse of a large value of either h or R_{56} in a low-emittance ring is overcome by disentangling bunch compression from the SRLS lattice, at the cost of installing two new arcs internally to the ring. We assume $\sigma_{\delta,0} = 0.08\%$ and $R_{56} = 0.2$ m in the arc; the minimum rms bunch duration, corresponding to an upright longitudinal phase space, is $\sigma_{z,\rm min} \approx R_{56}\sigma_{\delta,0} = 160$ μm. Since we also assume $\sigma_{z,0} \approx 2.7$ mm, the effective maximum compression factor results $C = \sigma_{z,0}/\sigma_{z,\rm min} \cong 16$.

We designed a compressive arc (CA, DA in Fig. 1) made of four triple bend achromatic cells. The arc total bending angle is $108°$. The arc length is chosen here to accommodate the FEL line along a diameter of the ring circumference. A different length can be chosen depending on the available space internally to the main ring.

A suitable choice of small betatron function in the dipoles and π-betatron phase advance between dipoles in the bending plane [37,38] minimizes the effect of coherent synchrotron radiation (CSR) on the horizontal emittance [39,40]. Sextupole magnets are distributed along the arc with the two-fold scope of keeping particles' longitudinal motion linear during compression, and of cancelling optical aberrations [41,42]. Similar lattice guidelines were followed to design the isochronous injection and extraction arc (IA, EA in Fig. 1). They include a shorter reverse bend in the middle of the cell. Optics functions are in Fig. 2 and lattice parameters are listed in Table II.

Each arc for bunch length manipulation is preceded or followed by an rf linac (see Fig. 1). According to Eq. (1), the energy chirp at maximum compression, $h = -1/R_{56}$, specifies the linac peak voltage at the phase of zero-crossing, $V = \lambda_{\rm rf}hE/(2\pi)$. Since each arc features $R_{56} = 0.2$ m in our design, a $\sim$120 MV peak voltage is required, for example, from each of the two normal conducting linacs for a rf chosen in C-band ($c/\lambda_{\rm rf} = 6$ GHz).

In general, an rf wavelength much longer than the stored bunches ensures more linear dynamics during compression, and therefore a possibly higher peak current at the TGU. S-band ($\sim$3 GHz) or L-band ($\sim$1.5 GHz) linacs might be considered for initial bunch durations longer than $\sim$20 ps rms, but at the expense of higher peak voltages. On the opposite, shorter bunches at equilibrium are compatible with higher frequency, lower peak voltage linacs. They also imply lower beam energy spread through the arcs for any given energy chirp, and therefore weaker chromatic aberrations.
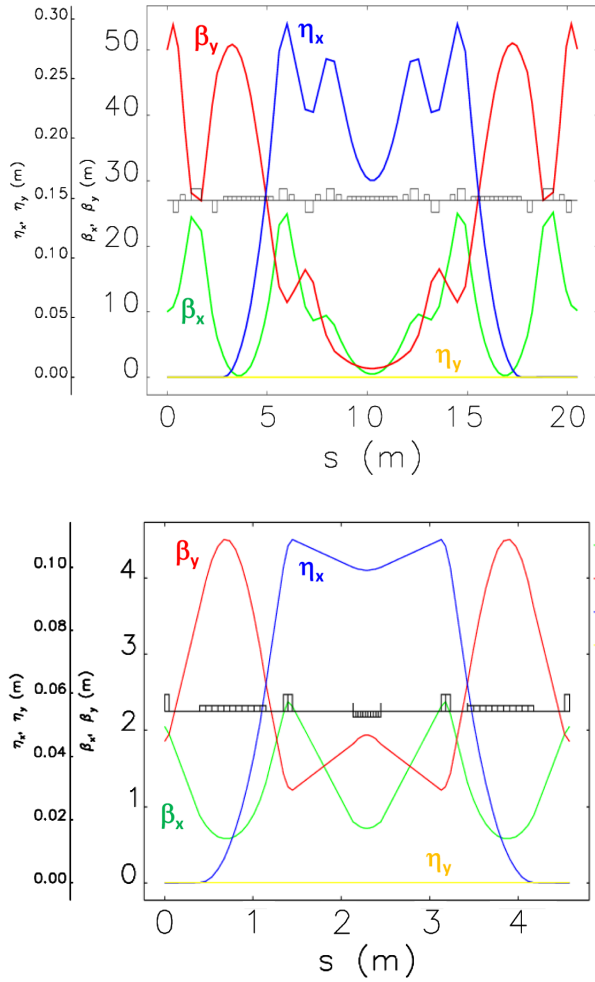
FIG. 2. Betatron and dispersion functions along one cell of the arc compressor (top; CA, DA in Fig. 1) and of the isochronous arc (bottom; IA, EA in Fig. 1). In gray, dipole (long small rectangles) and quadrupole magnets (short tall rectangles).

B. Particle tracking

To demonstrate proper control of the electron beam through the entire compression loop, particle tracking was carried out with the ELEGANT code [43] in the presence of third-order optical nonlinearities, rf curvature and geometric wakefields in the linacs, incoherent and coherent synchrotron radiation in the dipole magnets. Simulation results are shown in Figs. 3 and 4. Resulting beam parameters at the entrance of the TGU (exit of IA) are summarized in Table II.

At this stage, the effect of lasing through the TGU on the electrons' energy distribution is taken into account by gradually increasing the beam uncorrelated energy spread up to 0.1%; this is indeed the maximum FEL efficiency expected at saturation. Since the beam rms energy spread at the entrance of the TGU is approximately 1.3% (as a consequence of an initial energy spread of the stored beam around 0.08%, and bunch length compression by a factor 16 in the arc), the FEL perturbation to the energy

TABLE II. Parameters of magnetic arcs (CA, DA, IA, and EA in Fig. 1).

Arc section	CA	IA	Unit
Arc cell type	TBA	TBA	
Number of cells	4	5	
Total deflection angle	108	68.5	Deg
Total length	104	22.5	m
Dipole magnetic length	2.5	0.9, 0.4	m
Dipole magnetic field	0.63	1.8	T
Minimum horizontal betatron function	0.12	0.6	m
Maximum dispersion function	0.30	0.12	m
Correlated energy spread, rms	1.3	1.3	%
Total R_{56}, T_{566}	0.2, −0.07	0, 0.06	m
Compression factor	16	1	
Minimum bunch duration, rms	0.5	0.5	ps
Maximum peak current	712	712	A
Slice emittance @ arc end	270, 2	270, 2	pm

distribution is negligible on a single pass basis (see Fig. 3-top plot). Residual phase space nonlinearities appear at the bunch edges. Though not considered here, octupole magnets can be included in the arcs for further tuning of the longitudinal phase space during its apparent rotation.
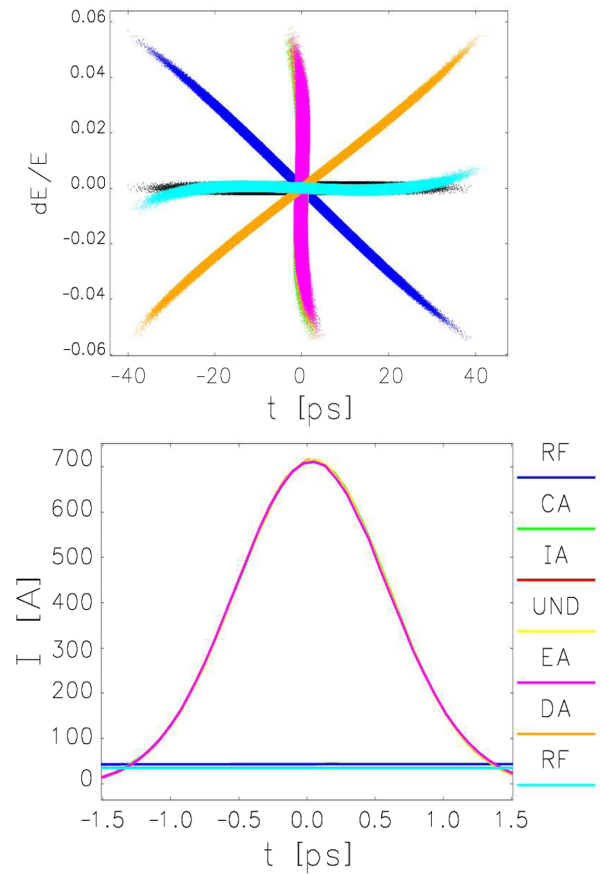
FIG. 3. Longitudinal phase space (top) and bunch peak current through one loop. The colored legend is the same in the two plots; labels refer to Fig. 1.
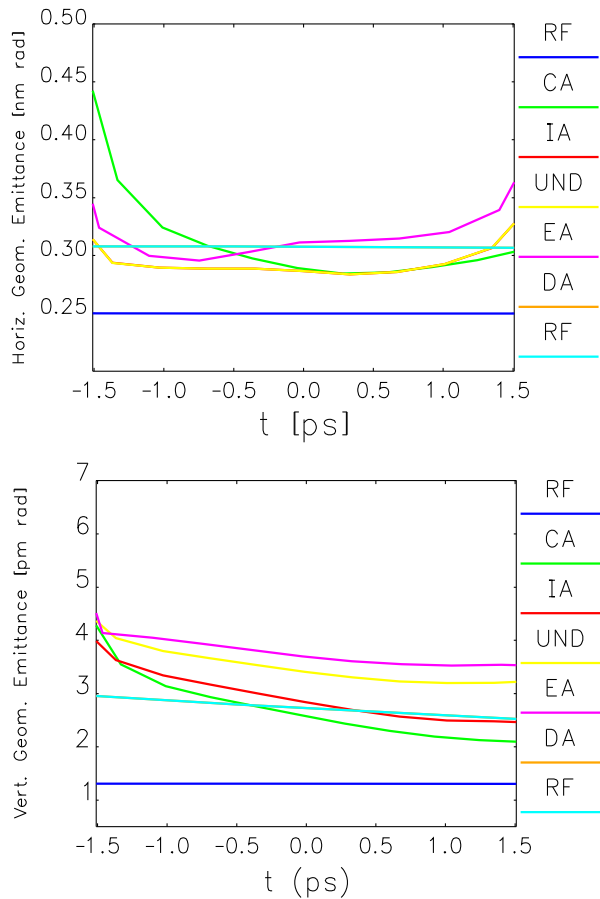
FIG. 4.   Slice geometric emittance in the bunch core through one loop; labels refer to Fig. 1. In the top plot, the yellow line (ε_x at the exit of TGU) is superimposed to the red line (exit of IA). In both plots, the cyan line ($\varepsilon_{x,y}$ at the loop end) is superimposed to the orange line (exit of decompressive arc).

Figure 4 depicts the slice emittance growth of the bunch core through one loop. An analysis of the tracking results for the horizontal plane of motion (top plot) shows that, at the point of full compression, particles belonging to different slices, therefore, subject to different CSR kicks and featuring different Courant-Snyder invariants, collapse into adjacent slices in the bunch core, whose emittance eventually increases (see e.g., blue and yellow line in the top plot). This effect is only partly recovered when the bunch is lengthened again. The slice emittance growth at the edges of the compressed bunch (green and violet line at $t = \pm 1.5$ ps) is mostly a numerical artifact due to the much lower number of particles in those regions compared to the core.

As a result, owing to residual CSR kicks and chromatic aberrations, the bend-plane emittance increases by $\Delta \varepsilon_x \cong$ 50 pm rad along one full loop (see blue and cyan line). In the vertical plane—Fig. 4-bottom plot—the slice emittance growth is dominated by residual optical aberrations in the arcs, and by particle energy change in the dispersive line of the TGU. Bunch lengthening redistributes the slice

emittance growth to some extent, and the vertical emittance increases by $\Delta \varepsilon_x \cong 1.5$ pm rad in one loop (see blue and cyan line).

One should now consider that ELEGANT tracking illustrates a pessimistic evolution of emittances through the loop, for at least two reasons. First, the one-dimensional approximation under which the CSR tail-head instability is modeled largely overestimates the emittance growth when the beam approaches full compression [44,45]. Second, multiobjective genetic algorithms applied to the sextupole strengths and positions, and not adopted here yet, would be ideally suited for canceling the effect of residual optical aberrations.

At the end, assuming more sophisticated nonlinear optics optimizations and three-dimensional CSR modeling in the arcs, a realistic emittance growth per loop $\Delta \varepsilon_x < 20$ pm rad (dominated by residual CSR effect, and largely independent from the initial emittance value) and $\Delta \varepsilon_y / \varepsilon_y < 50\%$ for initial value ε_y 1 pm rad [dominated by the chromatic effect in the TGU, see later Eq. (16)] can be expected.

It is worth reminding that after reinjection into the ring, and if the FEL repetition rate is small enough compared to the transverse damping time, the emittances shrink back to their equilibrium values. If lasing is frequent in a damping time, instead, some emittance growth will be accumulated until new equilibrium values are reached, as shown in Sec. VI.

IV. BEAM ENVELOPE TRACKING AND LASING

A. Longitudinal beam matrix

The existence of new equilibrium beam parameters in the SRLS, in the presence of single particle and beam collective effects such as synchrotron radiation in the storage ring, CSR in the compressors and lasing in the TGU, is not proven *a priori*. Massive particle tracking could in principle answer this question, following the electron beam longitudinal dynamics through the SR-HG-FEL for an arbitrary large number of passes. This, however, would amount to hundreds of thousands turns for few damping times only, and would therefore require an extremely intensive, if not prohibitive, simulation effort.

To overcome the computational challenge, which would also prevent any realistic optimization of the large number of parameters involved, we developed a matrix-based beam envelope tracking, so reducing the complexity of macro-particles simulations to the six-dimensional beam envelope in the configuration and momentum space. We simplified the modeling further by reducing the beam matrix to the longitudinal plane only. Modifications to the transverse emittances are then imposed as single-kick effect on the basis of particle tracking results (see Sec. III) and analytical evaluations [see later Eq. (16)].

The longitudinal beam matrix transforms through the SR-HG-FEL according to

$$M\Sigma M^t = \begin{pmatrix} \varepsilon_z\beta_z & -\varepsilon_z\alpha_z \\ -\varepsilon_z\alpha_z & \varepsilon_z\gamma_z \end{pmatrix}. \qquad (2)$$

Σ is defined in terms of second-order momenta of the beam particle longitudinal coordinate and energy deviation, β_z, α_z, and γ_z are the Courant-Snyder parameters for the particle longitudinal motion, and ε_z is the beam rms longitudinal emittance, where $\varepsilon_z^2 = \det|M\Sigma M^t|$. The bunch linear energy chirp required for compression in the arc is $z\delta/\sigma_z^2 = -\alpha_z/\beta_z$, and the beam total energy spread $\sigma_\delta^2 = \varepsilon_z(1+\alpha_z^2)/\beta_z = \sigma_{\delta,0}^2 + \sigma_{\delta,\text{cor}}^2$ is the quadratic sum of the uncorrelated and the z-correlated energy spread. M is the transport matrix of the whole beam line: It is the ordered product of 2×2 matrices describing the effect on beam energy spread and bunch duration, of rf linac and magnetic compression, lasing, synchrotron radiation damping, and quantum excitation.

The FEL output power at successive loops is calculated on the basis of the updated beam parameters at the undulator entrance. Doing so, bunch duration and energy spread can be calculated after an arbitrary large number of loops by applying *n*-times the single loop transport matrix to the initial beam envelope. In the following Secs. IV B–IV D, equations for the particle longitudinal and transverse dynamics in the SR-HG-FEL are derived and discussed. These will result in entries for the individual 2×2 transport matrices of the loop components, which are made explicit in Sec. IV E.

B. Longitudinal dynamics in the TGU

SASE FEL physics in a TGU is depicted in the one-dimensional approximation by means of the modified FEL parameter ρ_{TGU}, the FEL power gain length $L_{g,\text{TGU}}$, and the FEL power at saturation $P_{s,\text{TGU}}$. Their expression for a vertical undulator is [46]

$$L_{g,\text{TGU}} = \frac{\lambda_u}{4\pi\sqrt{3}\rho_{\text{TGU}}}\left[1+\left(\frac{\sigma_{\delta,ef}}{\rho_{\text{TGU}}}\right)^2\right],$$

$$\rho_{\text{TGU}} = \frac{\rho_{1D}}{[1+(\frac{\overline{\eta}_y\sigma_{\delta,u}}{\overline{\sigma}_{y,\beta}})^2]^{1/6}},$$

$$P_{S,\text{TGU}} = 1.6\rho_{\text{TGU}}P_e\left(\frac{\rho_{\text{TGU}}}{\rho_{1D}}\right)^2, \qquad (3)$$

where $\overline{\eta_y}$ and $\overline{\sigma_{y,\beta}}$ are the average value of vertical dispersion function and rms betatron beam size along the undulator, $\sigma_{\delta,u}$ is the beam rms relative energy spread at the undulator entrance, and $\sigma_{\delta,\text{eff}}^2 = \frac{\sigma_{\delta,u}^2}{1+(\overline{\eta}_y\sigma_{\delta,u}/\overline{\sigma}_{y,\beta})^2}$. In the approximation of preserved beam longitudinal emittance outside the TGU (as confirmed by particle tracking, see Sec. III), the beam uncorrelated energy spread at the undulator is simply $\sigma_{\delta,u}(t) = C\sigma_{\delta,0}(t)$, with $\sigma_{\delta,0}$ the uncor-related energy spread of the uncompressed beam in the

SRLS, and C is the total compression factor through the arc. The undulator length needed to reach saturation of the FEL power is $L_{s,\text{TGU}} = L_{g,\text{TGU}} \ln(9P_{s,\text{TGU}}/P_0)^2$.

The one-dimensional FEL parameter ρ_{1D} in Eq. (3) is [25]

$$\rho_{1D} = \frac{1}{2\gamma}\left(\frac{I}{I_A}\right)^{1/3}\left(\frac{\lambda_u a_w[JJ]}{2\pi\sigma_T}\right)^{2/3}, \qquad (4)$$

where I is the electron bunch peak current, $I_A = 17045$ A is the Alfven current, and $\sigma_T = \sqrt{\sigma_x^2+\sigma_y^2}$ is the quadratic sum of the electron beam rms transverse sizes. For a planar polarized undulator as in our baseline design, $[JJ] = [J_0(\xi)-J_1(\xi)]$, where J_0 and J_1 are Bessel's functions of the first kind with argument $\xi = K^2/(4+2K^2)$, $a_w = K/\sqrt{2}$, and $K \equiv eB_0\lambda_u/(2\pi m_e c) = 0.934B_0[\text{T}]\lambda_u[\text{cm}]$ is the so-called undulator parameter, B_0 is the undulator peak magnetic field, e and m_e are the electron charge and rest mass, respectively, and c is the speed of light in vacuum.

The FEL fundamental wavelength of emission is specified by the resonance condition:

$$\lambda = \frac{\lambda_u}{2\gamma^2}\left(1+\frac{K^2}{2}\right) \qquad (5)$$

and λ_u is the undulator period length.

The FEL-induced uncorrelated energy spread is evaluated by means of the logistic equation for the SASE FEL power P_{FEL} [47], but modified here for the TGU:

$$\sigma_{\delta,\text{FEL}}^2(n;z_u) \cong \frac{1.6\rho_{\text{TGU}}(n;z_u)P_{\text{FEL}}(n;z_u)}{P_e(n;z_u)}$$
$$= 1.6\rho_{\text{TGU}}\frac{P_0}{P_e}\frac{\exp(z/L_{g,\text{TGU}})}{1+\frac{P_0}{9P_{s,\text{TGU}}}\exp(z/L_{g,\text{TGU}})}, \qquad (6)$$

where n runs over the FEL loop number, z_u runs along the undulator, and we discarded the $(n;z)$ notation in the rhs of Eq. (6) for brevity. $P_e = EI/e$ is the electron bunch peak power and $P_0 = \sqrt{2\pi}ce\rho_{\text{TGU}}^2E/\lambda$ estimates the electron beam shot noise power at the undulator entrance.

Equation (6) is able to capture the time evolution of $\sigma_{\delta,\text{FEL}}$ in the exponential regime of power amplification, up to saturation. The undulator length is a free parameter that, within the geometrical constrain given by the SRLS size, can be optimized for tuning the FEL performance vs the FEL-induced energy spread. In the following, a TGU length of ~70 m is shown to safely guarantee power saturation for lasing in single pass mode, at photon energies around 100 eV.

C. Longitudinal dynamics in the SRLS

Modeling of longitudinal particle motion in a SRLS starts from the educated assumption of a damped oscillation

of particle's energy deviation δ and longitudinal position z, both defined with respect to the synchronous particle. With values δ_{in} and θ_{in} at injection in the SRLS, we have

$$\delta(t) = \delta_{in} e^{-\frac{t}{\tau_E}} \sin(\omega_s t + \theta_{in}),$$

$$z(t) = \frac{\alpha_c c}{\omega_s} \delta_{in} e^{-\frac{t}{\tau_E}} \cos(\omega_s t + \theta_{in}). \quad (7)$$

τ_E is the longitudinal damping time and ω_s is the synchrotron angular frequency. The beam rms longitudinal emittance is

$$\varepsilon_z(t) = \sqrt{\overline{\delta(t)^2 z(t)^2} - \overline{\delta(t) z(t)}}$$

$$\cong \left(\frac{\alpha_c c}{\omega_s}\right) \sigma_{\delta,in}^2 e^{-\frac{2t}{\tau_E}} \equiv \varepsilon_{z,0} e^{-\frac{2t}{\tau_E}}, \quad (8)$$

where the average is intended over the beam particles distribution, and no correlation of the longitudinal coordinates is initially present. $\varepsilon_{z,0}$ is the emittance value at time $t = 0$ and, in general, it is far from equilibrium.

In order to describe an equilibrium condition for the emittance at times $t \gg \tau_E$, Eq. (8) has to be revised so as to provide the solution $\varepsilon_z(t) = \varepsilon_{z,eq}$ when the stationary condition $\frac{d\varepsilon_z(t)}{dt} = 0$ is imposed. Our *ansatz* is

$$\varepsilon_z(t) = \varepsilon_{z,0} e^{-\frac{2t}{\tau_E}} + \varepsilon_{z,eq}(1 - e^{-\frac{2t}{\tau_E}}). \quad (9)$$

Its first time derivative gives

$$\frac{d\varepsilon_z(t)}{dt} = -\frac{2}{\tau_E}(\varepsilon_{z,0} - \varepsilon_{z,eq}) e^{-\frac{2t}{\tau_E}} = \frac{2}{\tau_E}(\varepsilon_{z,eq} - \varepsilon_z(t)) \quad (10)$$

Equation (10) applies identically to the second-order moment of the energy distribution (we assume a distribution with zero-average momentum deviation):

$$\frac{d\sigma_\delta^2(t)}{dt} = \frac{2}{\tau_E}(\sigma_{\delta,eq}^2 - \sigma_\delta^2(t)), \quad (11)$$

whose solution is

$$\sigma_\delta^2(t) = \sigma_{\delta,in}^2(t) e^{-\frac{2t}{\tau_E}} + \sigma_{\delta,eq}^2(1 - e^{-\frac{2t}{\tau_E}}). \quad (12)$$

The variation of beam energy spread due to synchrotron radiation damping, averaged over one revolution period T_0, is calculated from Eq. 11 for the ith turn:

$$\frac{d\sigma_{\delta,i+1}^2(t)}{dt}\bigg|_{T_0} = -\frac{2}{\tau_E}\sigma_{\delta,i}^2. \quad (13)$$

This allows us to write the energy spread after one turn

$$d\sigma_{\delta,i+1}^2(T_0) = \sigma_{\delta,i+1}^2(T_0) - \sigma_{\delta,i}^2 = -\frac{2T_0}{\tau_E}\sigma_{\delta,i}^2,$$

$$\Rightarrow \sigma_{\delta,i+1}^2(T_0) = \left(1 - \frac{2T_0}{\tau_E}\right)\sigma_{\delta,i}^2. \quad (14)$$

At equilibrium, the effect of quantum excitation balances the effect of radiation damping. So, the one-turn antidamping beam matrix must add to the incoming beam matrix and eventually result in the equilibrium value for the energy spread. Equation (14) is therefore modified as follows:

$$\sigma_{\delta,i+1}^2(T_0) = \left(1 - \frac{2T_0}{\tau_E}\right)\sigma_{\delta,i}^2 + A_{22}(\sigma_{\delta,i}^2) \equiv \sigma_{\delta,eq}^2, \quad (15)$$

with A_{22}, the element of the beam matrix describing the effect of quantum excitation.

D. Transverse emittance

The matrix M contains information on the beam transverse emittance through the FEL parameter, which depends in turn on the beam transverse size $\sigma_{x,y}$, see Eqs. (3) and (4). As anticipated in Sec. III, the vertical emittance growth is largely dominated by the effect of lasing in the presence of vertical dispersion. Such growth is an incoherent effect and its upper limit at the ith pass through the undulator is estimated by assuming full filamentation in the vertical phase space:

$$\varepsilon_{y,i}^2 \approx \varepsilon_{y,i-1}^2 \left[1 + \frac{(\bar{\eta}_y \sigma_{\delta,FEL})^2}{\varepsilon_{y,i-1}\bar{\beta}_y}\right]. \quad (16)$$

When $T_{FEL}/\tau_E \gg 1$, the FEL can reach saturation at every pass so that $\sigma_{\delta,FEL} \approx 1.6\rho_{TGU} \le 0.1\%$. Consequently, the initial ~ 1 pm rad vertical emittance can increase up to threefold for practical values $\overline{\eta_y} \approx 15$ mm and $\overline{\beta_y} \approx 10$ m. This is in reasonable agreement with particle tracking results (see Fig. 4). But, since this growth would only reflect into a 1.7 times larger geometric beam size, the total beam size remains dominated by the particle chromatic motion, and electrons remain on-resonance in the TGU. In between successive lasing, the initial equilibrium emittance value is recovered in the SRLS in one transverse damping time or so.

When $T_{FEL}/\tau_E \le 1$ instead, the emittance growth collected during the very first passage through the TGU is not recovered anymore, and it may lead to a strong reduction of the FEL gain at successive loops. The rate of vertical emittance growth, averaged over one loop, is

$$\frac{d\varepsilon_y}{dt}\bigg|_{FEL} \approx \frac{1}{T_{FEL}}\frac{(\bar{\eta}_y \sigma_{\delta,FEL})^2}{2\bar{\beta}_y} \equiv \frac{\varepsilon_{y,eq}}{\tau_y} \cong \frac{\kappa \varepsilon_{x,eq}}{\tau_y}, \quad (17)$$

with κ, the geometric coupling coefficient, and τ_y is the vertical damping time. For example, in order for the vertical emittance not to triple at equilibrium, and therefore the gain length not to be enlarged by more than $\sim 20\%$, the repetition rate of a lasing bunch has to satisfy $T_{FEL} \ge 700$ μs, i.e., the same bunches are allowed to lase every ~ 400 turns or more (1.4 kHz repetition rate or lower).

In summary, slice emittance growth in the transverse planes is taken into account by updating the emittance value at successive loops by means of amplification factors estimated in Sec. III, which describe the effect of residual CSR tail-head instability in the horizontal plane, radiation emission in the TGU for the vertical plane, and residual optical aberrations in the arcs.

The updated emittance value is cast into the definition of ρ_{1D} and ρ_{TGU} [Eqs. (3) and (4)] at every loop. The rough agreement of particle tracking results in Fig. 4 and theoretical estimations through Eq. (16) confirm that the vertical emittance growth in the TGU is the major limitation for a SR-HG-FEL to lase at wavelengths in the EUV range (or shorter) and at high-repetition rates.

The emittance degradation can be partially alleviated by a coupling coefficient pushed on purpose to the level of 10% or larger (not considered here). For lasing in single pass mode, the reduction in FEL power due to emittance growth can be compensated, to some extent, by a reasonably longer undulator.

E. Beam matrix transformation including lasing

The loop depicted in Fig. 1 starts with beam extraction from the SRLS. A linear energy chirp is imparted to the beam by the first linac, according to the matrix:

$$H = \begin{pmatrix} 1 & 0 \\ h & 1 \end{pmatrix}. \tag{18}$$

Bunch length is then compressed in the arc via

$$R = \begin{pmatrix} 1 & R_{56} \\ 0 & 1 \end{pmatrix}. \tag{19}$$

Matrices R and H apply identically at the exit of the TGU. Since the beam reaches the TGU at full compression, they produce bunch lengthening and energy chirp removal (see Fig. 3). The product matrix of the compression-decompression process describes a full beam rotation in the longitudinal phase space when $R_{56} = -h^{-1}$. But, since it is not a unitary matrix, some distortions to the phase space might show up if the full matrix is applied many consecutive times.

In fact, the matrix can be approximated to an identity transformation as long as $R_{56}\sigma_{\delta,0} \ll \sigma_{z,0}$, which is satisfied in our case (see Tables I and II). Still, an exact unitary matrix for the bunch gymnastic does not prevent the phase space from filamentation: Higher order nonlinearities, for example, due to rf curvature in the linacs and nonlinear momentum compaction in the arcs, can perturb the longitudinal emittance. Such nonlinearities are compensated with a suitable setting of the sextupole and octupole magnets, as discussed in Sec. III.

The beam matrix at the TGU exit is given by that one at the undulator entrance with the addition of the

FEL-induced energy spread (bunch length is frozen in the undulator):

$$F = \begin{pmatrix} 1 & 0 \\ 0 & \sigma_{\delta,\text{FEL}}^2 \end{pmatrix}, \tag{20}$$

and $\sigma_{\delta,\text{FEL}}$ is given by Eq. (6). As prescribed in Ref. [46], we consider a 15% longer $L_{g,\text{TGU}}$ in the definition of $\sigma_{\delta,\text{FEL}}$, in order to mimic three-dimensional effects such as asymmetric electron beam sizes.

Once stored again in the ring, the electron beam is subject to longitudinal rf focusing, which replenishes the beam energy loss due to emission of synchrotron radiation. The one-turn transport matrix for rf focusing is

$$P = \begin{pmatrix} 1 & 0 \\ k_{\text{rf}} & 1 \end{pmatrix}, \tag{21}$$

with $k_{\text{rf}} = 2\pi V_{\text{rf}} \cos\varphi_{\text{rf}}/(E\lambda_{\text{rf}})$, and V_{rf} typically in the 1–3 MV range.

The effect of the SRLS momentum compaction is represented by

$$S = \begin{pmatrix} 1 & R_{56,S} \\ 0 & 1 \end{pmatrix}. \tag{22}$$

The effect of one-turn radiation damping on the beam energy spread is described by Eq. (14), and the associated transport matrix is

$$D = \begin{pmatrix} 1 & 0 \\ 0 & \sqrt{1 - \frac{2T_0}{\tau_E}} \end{pmatrix}. \tag{23}$$

Finally, the increase of beam energy spread due to the one-turn quantum excitation is depicted by a matrix which, according to Eq. (15), adds to the incoming beam matrix Σ:

$$A = \begin{pmatrix} 0 & 0 \\ 0 & \frac{2T_0}{\tau_E}\sigma_{\delta,i}^2 \end{pmatrix}. \tag{24}$$

By virtue of Eqs. (18)–(24), the beam matrix transforms through the ith SR-HG-FEL loop as follows:

$$\Sigma_{F,i} = (R \cdot H \cdot P)\Sigma_{A,i-1}(R \cdot H \cdot P)^t + F_{i-1},$$
$$\Sigma_{A,i} = (P \cdot D \cdot S \cdot H \cdot R)\Sigma_{F,i}(P \cdot D \cdot S \cdot H \cdot R)^t + A. \tag{25}$$

$\Sigma_{A,i-1}$ is the beam matrix of the stored beam at the end of the $(i-1)$th loop; $\Sigma_{F,i}$ is at the end of undulator in the ith loop.

Matrices P, H, R, and S are simplectic, therefore, they imply preservation of beam emittance (Liouvillian behavior). Matrix D (radiation damping) is not symplectic, but its one-turn average effect on the emittance is "compensated"

by the effect of matrix A (quantum excitation). Matrix F (lasing) shifts the equilibrium emittance far from its unperturbed value.

The nonunitary matrix F corresponds to an additional driving term in Eq. (11) for the beam relative energy spread in the SRLS. In the presence of lasing, Eq. (11) now reads

$$\frac{d\sigma_\delta^2(t)}{dt} = \frac{2}{\tau_E}(\sigma_{\delta,0}^2 - \sigma_\delta^2(t)) + \frac{\sigma_{\delta,\text{FEL}}^2(t)}{C^2 T_{\text{FEL}}}. \qquad (26)$$

We remind that the rms energy spread σ_δ is the one of the beam stored in the SRLS after lasing, and $\sigma_{\delta,0}$ is the rms energy spread at equilibrium without lasing. The timescale to reach equilibrium is the longitudinal damping time τ_E15 ms. $\sigma_{\delta,\text{FEL}}$, averaged over one lasing period T_{FEL}, acts as a driving term, shifting the equilibrium energy spread to a new working point.

When the bunch is reinjected into the SRLS, $\sigma_{\delta,\text{FEL}}$ is C-times smaller because of the (approximate) preservation of the longitudinal emittance during bunch lengthening. The appearance of C in Eq. (26) shows the advantage of nonequilibrium compression in reducing the FEL perturbation to the beam dynamics. This is elucidated further in Sec. V.

V. BEAM AND FEL AT EQUILIBRIUM

A. Bunch current and energy spread

Electron beam and FEL parameters are predicted by iterating Eq. (25) over an arbitrary number of loops. Before going through that, an analytical insight into the temporal evolution of the bunch peak current and energy spread is given below. In the following, we adopt the subscript index "1" for beam stored in the ring, "2" for beam after compression, "3" after lasing, and "4" for the decompressed beam reinjected into the ring.

In the approximation of linear longitudinal motion and preservation of longitudinal emittance in the arcs, the bunch length at the point of full compression is $\sigma_{z,2} = R_{56}\sigma_{\delta,1}$, with $\sigma_{\delta,1}$ the initial uncorrelated relative energy spread. The bunch length after lasing and decompression is

$$\sigma_{z,4} = R_{56}\sigma_{\delta,3} = R_{56}\sqrt{\sigma_{\delta,2}^2 + \sigma_{\delta,\text{FEL}}^2}$$
$$= R_{56}\sqrt{C_{1,2}^2\sigma_{\delta,1}^2 + \sigma_{\delta,\text{FEL}}^2}, \qquad (27)$$

where

$$C_{1,2} = \frac{\sigma_{z,1}}{\sigma_{z,2}} = \frac{\sigma_{\delta,2}}{\sigma_{\delta,1}} = \frac{\sigma_{z,1}}{R_{56}\sigma_{\delta,1}} \qquad (28)$$

is the linear bunch length compression factor. Making use of Eqs. (27) and (28), the ratio of the stored bunch peak current after and before one loop results:

$$\frac{I_4}{I_1} = \frac{\sigma_{z,1}}{\sigma_{z,4}} = \frac{C_{1,2}\sigma_{z,2}}{R_{56}\sqrt{C_{1,2}^2\sigma_{\delta,1}^2 + \sigma_{\delta,\text{FEL}}^2}}$$
$$= \frac{C_{1,2}R_{56}\sigma_{\delta,1}}{R_{56}\sqrt{C_{1,2}^2\sigma_{\delta,1}^2 + \sigma_{\delta,\text{FEL}}^2}} = \frac{\sigma_{\delta,2}}{\sigma_{\delta,3}}. \qquad (29)$$

Equation (29) says that, as expected, the FEL-induced energy spread contributes to bunch lengthening only once the beam is decompressed and reinjected into the SRLS.

Equation (29) can also be cast in the form

$$\frac{I_4}{I_1} = \frac{C_{1,2}\sigma_{\delta,1}}{\sqrt{C_{1,2}^2\sigma_{\delta,1}^2 + \sigma_{\delta,\text{FEL}}^2}} = \frac{\sigma_{\delta,1}}{\sqrt{\sigma_{\delta,1}^2 + \sigma_{\delta,\text{FEL}}^2/C_{1,2}^2}}, \qquad (30)$$

which shows that, compared to a situation without bunch compression, the proposed scheme minimizes the impact of FEL on the energy spread of the stored beam, and therefore on the compressed peak current, by just the compression factor.

Once the interplay of radiation damping, quantum excitation, and lasing have led to equilibrium beam parameters, Eq. (28) becomes

$$C_{\text{eq}} = \frac{\sigma_{z,\text{eq}}}{R_{56}\sigma_{\delta,\text{eq}}} \propto \frac{\sigma_{\delta,\text{eq}}}{R_{56}\sigma_{\delta,\text{eq}}} \propto \frac{1}{R_{56}}. \qquad (31)$$

Namely, the compression factor is constant and, in particular, it does not depend on the beam energy spread at equilibrium. The bunch peak current at the undulator becomes

$$I_{2,\text{eq}} = C_{\text{eq}}I_{1,\text{eq}} \propto \frac{C_{\text{eq}}}{\sigma_{z,\text{eq}}} \propto \frac{C_{\text{eq}}}{\sigma_{\delta,\text{eq}}}. \qquad (32)$$

We note that the inverse linear dependence of the peak current on the energy spread at equilibrium was also assumed in Ref. [19] without derivation.

If I_0 and $\sigma_{\delta,0}$ are the peak current and the energy spread at the entrance of the undulator at the very first pass, then the peak current at the undulator at the generic time t reads

$$\frac{I(t)}{I_0} = \frac{\sigma_{\delta,0}}{\sigma_{\delta(t)}}. \qquad (33)$$

By virtue of Eq. (4), it implies

$$\rho_{1D}(t) = \rho_0\left[\frac{\sigma_{\delta,0}}{\sigma_{\delta(t)}}\right]^{1/3}, \qquad (34)$$

with ρ_0, the FEL parameter at the very first lasing. Equations (32) and (34) say that, as the beam longitudinal emittance will have reached equilibrium, also the FEL output power will be constant at every lasing.

B. FEL peak power

We now demonstrate that, if lasing occurs frequently in a damping time, the SASE FEL power never saturates at equilibrium, no matters how long the undulator is. In other words, the tendency of the SR-HG-FEL towards a new equilibrium of the beam parameters shifts, turn by turn, the FEL saturation length over any undulator length initially given.

At first, we follow the reasoning introduced in Ref. [19]. In order for the FEL-induced energy spread to be fully damped by emission of synchrotron radiation over one turn, its value, properly diminished by the compression factor in our scheme, should be comparable to the energy diffusion from quantum excitation:

$$\frac{\sigma_{\delta,0}^2}{\tau_E} \equiv \frac{\sigma_{\delta,\mathrm{FEL}}^2}{C_0^2 T_{\mathrm{FEL}}} \approx \frac{\rho_{\mathrm{TGU}} \hat{P}_{\mathrm{FEL}}}{C_0^2 T_{\mathrm{FEL}} P_e} \qquad (35)$$

The FEL peak power can be estimated as

$$\hat{P}_{\mathrm{FEL}} \approx \rho_{\mathrm{TGU}} P_e \left(C_0^2 \frac{T_{\mathrm{FEL}}}{\tau_E} \right) \approx P_{s,\mathrm{TGU}} \left(C_0^2 \frac{T_{\mathrm{FEL}}}{\tau_E} \right), \quad (36)$$

where we used $\rho_{\mathrm{TGU}} \approx \sigma_{\delta,0}$. It turns out that the maximum FEL power $\hat{P}_{\mathrm{FEL}}$ at equilibrium is always smaller than the saturation power. For example, the diminishing factor is in the range 0.01–0.1 for $C_0 \sim 10$, $\tau_E \sim 10$ ms, and $T_{\mathrm{FEL}} < 100$ μs. The physical meaning of a short T_{FEL} is a high- FEL pulse repetition rate, obtained at the expense of low peak power. On the opposite, longer T_{FEL} imply that the effect of the FEL on the beam energy spread is washed out by radiation damping between two consecutive lasing, the FEL behaves as a single pass system and Eq. (36) does not apply anymore.

In summary, even if the undulator length L_u is longer than the saturation length $L_{S,\mathrm{TGU}}$ during the very first loops, very frequent lasing induces more and more energy spread, which translates into longer and longer stored bunches, until the bunch peak current is so low [see Eq. (32)] that saturation is not achieved anymore. Nonetheless, by virtue of nonequilibrium compression, the ratio $\hat{P}_{\mathrm{FEL}}/P_{s,\mathrm{TGU}}$ is increased by up to two orders of magnitude with respect to the case of uncompressed beams, for which the FEL peak power was shown not to exceed ~0.1% of the equivalent single-pass FEL power at saturation [19].

VI. TRACKING RESULTS

In this section, beam envelope tracking is compared with particle tracking results and FEL simulations. These are obtained from ELEGANT runs for the accelerator, concatenated to three-dimensional time-dependent FEL simulations in the TGU done with a modified version of GENESIS [48]. The benchmarking applies to a single pass through the loop in Fig. 1. The agreement of the two techniques is a solid basis for the extension of envelope tracking to a multiturn scenario, i.e., to an arbitrary number of loops per damping time. In the following, two sets of TGU parameters are shown, which match the resonant wavelength of 4 and 13 nm (intermediate wavelengths were investigated, but not shown for brevity).

A. Undulator

The electron beam is assumed to wiggle in the TGU in the vertical plane, in the presence of vertical energy dispersion, because its ultralow vertical emittance maximizes ρ_{TGU} [see Eq. (3)]. Although a technical design of the TGU is out of the aim of this article, we still assess the feasibility of a planar, vertically polarized undulator based on state-of-the-art technology. We assume an Apple-X configuration of the magnetic arrays [49,50]. The magnetic and the pole material of the PM hybrid undulator are, for example, like in the LCLS-II design [51]. The period length is chosen in the range 30–40 mm, and the undulator parameter in the range $K = 4$–6.5 for lasing between 4 and 13 nm. A minimum full gap of ~6 mm is expected for the highest K. A similar set of parameters for lasing at 13.5 nm has recently been considered in Ref. [52].

A vertical field gradient $\alpha = \frac{\Delta K}{\Delta y} \approx 85$ m^{-1} is generated on axis. It matches an energy dispersion function $\eta_y \approx 13$ mm [46,53], which is generated at the end of IA by a short vertical dogleg. Since no quadrupole magnets are embedded in the undulator line, the dispersion is constant through the TGU, and it dominates the vertical beam size $\sigma_y \approx \eta_y \sigma_\delta < 180$ μm. The vertical betatron function is minimized along the undulator and its average value is approximately 50 m.

The horizontal beam size, only due to the betatron motion, is kept to less than 70 μm by the TGU natural focusing. Worth to mention, the vertical doglegs at the TGU ends put the FEL beamline at a different height than the SRLS, so avoiding possible interference.

In the following, two distinct sets of TGU parameters are used for tracking (see Table III), optimized, respectively, for 4 and 13 nm. A single set of parameters corresponding to the longer period of 40 mm could be used in principle, but with an estimated reduction of the FEL power at saturation by approximately 20% at 4 nm. Superconducting undulators are an alternative suitable choice for periods shorter than 40 mm and still very high field as in our needs. Their performance is commonly traded off with technical complexity and operational costs.

B. Single-pass FEL

FEL is generated in single pass mode when an electron bunch lases at time periods longer than one longitudinal damping time. Under this assumption, Eqs. (3)–(5) predict a net total undulator length shorter than 70 m in order to

TABLE III. FEL parameters for lasing at 13 and 4 nm in single pass mode, predicted by beam envelope tracking and, in parenthesis, by GENESIS. The average FEL power is the product of the single pulse energy and the bunch repetition rate of 2.5 kHz (e.g., a train of 25 bunches injected in the bypass at 100 Hz).

FEL Wavelength	13	4	nm
Beam energy		3	GeV
Bunch charge		1	nC
Peak current		715	A
Energy spread, rms		1.4	%
Transverse emittance		270, 3.5	pm
Undulator length		80	m
Undulator period	40	30	mm
Undulator parameter	6.5	4.1	
Field gradient		85	m^{-1}
Vertical dispersion		13	mm
Average beam size (x, y)		∼80, ∼170	mm
FEL parameter	0.12	0.07	%
Gain length	2.7 (3.1)	2.9 (3.0)	m
Pulse duration, rms		∼0.4 (∼0.5)	ps
Peak power@Satur.	0.42 (0.20)	0.26 (0.28)	GW
Energy/pulse@Satur.	0.26 (0.21)	0.15 (0.14)	mJ
Repetition rate		2.5	kHz
Average total power	0.7 (0.5)	0.4 (0.4)	W

FIG. 5. SASE FEL peak power along the TGU in single pass mode, from GENESIS runs at the wavelength of 13 nm (top) and 4 nm (bottom). Each curve is the average of an ensemble of runs starting from random noise seed. Electron beam and FEL parameters are in Tables I and III. The dotted dashed black line guides the eye along the exponential power growth. The dotted green lines (dashed red lines) point to the end of the exponential growth in GENESIS (saturation in beam envelope tracking).

safely reach saturation at fundamental wavelengths in the range 4–13 nm.

A TGU line made of 35, 2.5 m long-undulator segments was modeled in GENESIS. A systematic comparison of beam envelope tracking and GENESIS simulations at the wavelengths of 4, 7, and 13 nm indicates a stronger deviation of the two codes at longer wavelengths, with a maximum discrepancy of 15% in saturation length, and up to a factor 2 in power at saturation, see Fig. 5. The discrepancy is attributed to several reasons.

First, envelope tracking assumes constant beam sizes along the undulator, whereas in GENESIS the vertical betatron size varies along the undulator by up to 40%, and the horizontal one by ∼20%. Second, beam envelope tracking assumes a perfectly matched resonance condition along the undulator, whereas the actual beam energy distribution tends to escape the energy matching due to energy loss (no tapering is applied to the simulations). Third, the bunch edges of the Gaussian current distribution contribute less to the FEL emission in the first part of the undulator because of their lower current. Those electrons tend to remain energy-matched to the TGU for a longer time, and to emit partly coherent radiation even when the bunch core is fully energy-saturated. This explains a quadratic growth of the peak power at undulator distances exceeding 60 m. Finally, three-dimensional diffraction effects are taken into account in the envelope tracking roughly, by artificially increasing the predicted one-dimensional gain length by 15%.

According to this picture, we have defined the saturation length in GENESIS, and the associated FEL power at

saturation, in correspondence of the undulator distance where the power growth starts deviating from the exponential behavior.

The discrepancy between the two models is much smaller for the FEL pulse energy. In the envelope tracking, a factor 0.6 is applied to the product of peak power and FWHM bunch duration, to take into account the spiky nature of SASE emission. In GENESIS, the pulse energy is calculated as the integral of the spectral power distribution. In the wavelength range 4–13 nm, the maximum discrepancy in pulse energy at the point of power saturation is always smaller than 20%. Figure 6 shows a representative plot of the SASE power distribution along the pulse, and the transverse intensity distribution at the undulator distance of 80 m, for lasing at 13 nm.

C. Multipass FEL

Lasing from a single bunch at high-repetition rates is now discussed. The initial beam matrix in Eq. (2) is defined for the unperturbed bunch with $z\delta = 0$. Then, Eq. (25) is
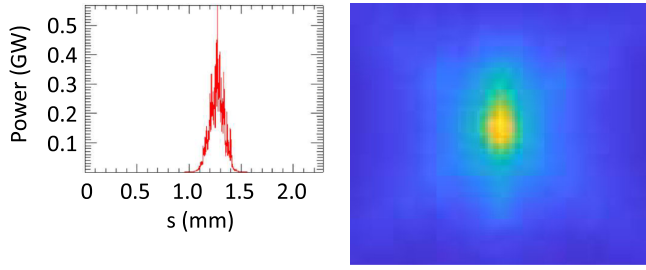
FIG. 6. Power distribution along pulse (left) and transverse intensity distribution, representative of SASE at 13 nm, after 80 m in the TGU. The square size is $50 \, \mu m \times 50 \, \mu m$.

used to track the longitudinal beam envelope through the FEL loop. At each loop, bunch length, uncorrelated energy spread, and other relevant beam parameters are recorded.

Figures 7 and 8 illustrate the time evolution in inverse longitudinal damping time, of the electron beam longitudinal and vertical emittance in the SRLS, of the FEL saturation length, and the FEL output power after 80 m in the TGU, at the fundamental wavelength of 4 nm. We present results for a high- and a moderate- single bunch repetition rate, corresponding to $T_{\text{FEL}}/\tau_E \approx 0.05\%$ and 10%, respectively, i.e., lasing from same bunch every 2.5 turns (227 kHz) and 570 turns (1 kHz).

At 227 kHz, the FEL gain is largely reduced by the vertical emittance growth already after few passes in the by-pass. The fast reduction of the FEL peak power eventually leads to minimal perturbation to the electron beam parameters in the SRLS, so that a new equilibrium state is reached within a fraction of the longitudinal damping time.

Lasing at 1 kHz shows some dynamics of both electron beam and FEL parameters, being it an intermediate
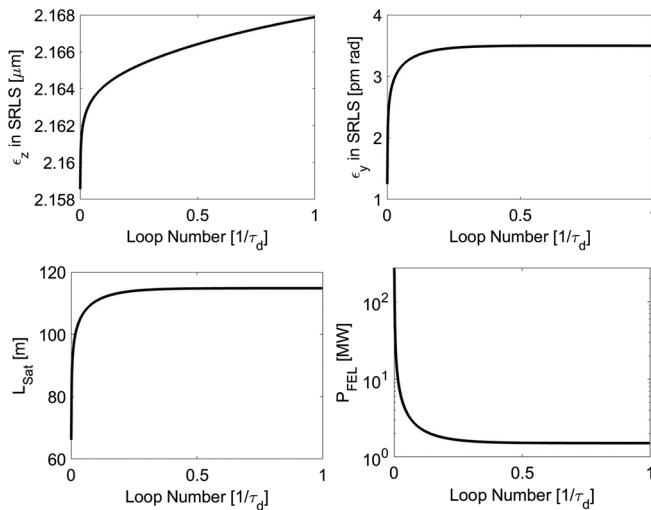
FIG. 7. From top-left to bottom-right: Electron beam longitudinal emittance and geometric vertical emittance in the SRLS, FEL saturation length and peak power out of an 80 m-long TGU, vs number of loops in units of longitudinal damping time. The FEL wavelength is 4 nm. The same bunch is lasing every 2.5 turns in the SRLS (227 kHz).
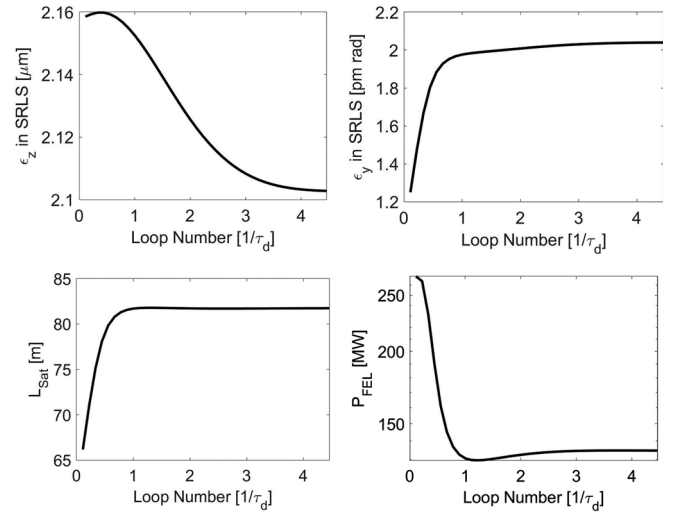
FIG. 8. Same quantities as in Fig. 7, but now the same bunch is lasing every 570 turns in the SRLS (1 kHz).

scenario between single-pass and very frequent lasing. The equilibrium is reached in three damping times or so. The time spent by the bunch in the SRLS is enough to partly wash out the FEL-induced energy spread and emittance growth. As a result, relatively high peak power pulses are emitted in the TGU, close to saturation.

Table IV summarizes the FEL single pulse performance at 4 nm in single-pass (0.1 kHz) and multipass mode (1 and

TABLE IV. SR-HG-FEL parameters *at equilibrium*, for lasing at 4 nm in single and multipass mode, predicted by beam envelope tracking.

Kicker repetition Rate	0.1	1	227	kHz
Linac parameters				
rf technology	NC	NC	SC	
rf frequency	6	6	1.5	GHz
Linac peak voltage	120	120	480	MeV
Linac repetition rate	0.1	1	1000	kHz
Accelerating gradient	35	12	30	MV/m
Linac length	3	10	16	m
Beam parameters				
Relative energy spread	0.08	0.08	0.08	%
Bunch duration, rms	9	9	9	ps
Emittance (x, y)	250, 1	280, 2	330, 3.5	pm
FEL parameters				
Undulator length	80	80	80	m
FEL parameter	0.06	0.07	0.07	%
Saturation length	66	82	116	m
Peak power/pulse	260	134	1.5	MW
Pulse duration, rms	0.5	0.5	0.5	ps
Pulse energy	~150	~75	~1	μJ
Pulses per train	25	50	50	
FEL Repetition Rate	2.5	50	11×10^3	kHz
Average total power	0.4	3.8	11	W

227 kHz). Linac parameters are anticipated on the basis of Eq. (1) (see also Sec. VII B). In all cases, the equilibrium state of the beam corresponds to an FEL steady-state emission, in confirmation of the theoretical findings in Sec. V.

VII. FEL REPETITION RATE

A. Injection and extraction system

For beam injection into, and extraction from the bypass, we consider the on axis swap-out scheme [29]. A series of stripline kickers provide a total bending angle of ∼1 mrad. They are surrounded by a pair of thin septum magnets, for a total deflection of approximately 60 mrad, as shown in Fig. 9. The system can be accommodated in 5 m.

The first option in Table IV at 0.1 kHz kicker repetition rate relies, for example, on tapered stripline kickers as used at the DAPHNE electron-positron collider [54]. By scaling the existing kicker parameters to 3 GeV beam energy, the total deflection angle turns out to be 0.8 mrad. We assume a flat-top pulse duration of 50 ns, rise and fall time of ∼10 ns. A train of 25 bunches and internal spacing of 2 ns is kicked into the bypass and, after 0.88 μs, it is reinjected into a 50 ns-long train of empty buckets. The rest of the ring can be filled uniformly, and the ring filling pattern can be maximized to 95% (see Fig. 1).

The second option at 1 kHz kicker repetition rate is inspired to the design in Refs. [55,56], here with flat-top pulse duration extended to 100 ns to accommodate up to 50 bunches, but at a repetition rate much lower than in original design.

The third option pushes the kickers' parameters to the horizon of present technology, see for example [57]. Instead of the proposed ∼1 MHz repetition rate in burst mode, we assume a continuous operation at 227 kHz, and a kicker flat-top pulse duration extended to 100 ns (an analogous fast "camshaft" bunch kicker is used at the Advanced Light Source at higher rates but kick angle lower than 1 mrad [58,59]).

The kickers must be synchronized with subnanosecond accuracy to the arrival time of the bunch(es) selected for lasing. After lasing, the decompressed and dechirped bunch encounters a mirrored septum system which injects the beam onto the ring axis with a residual ∼1 mrad angle.
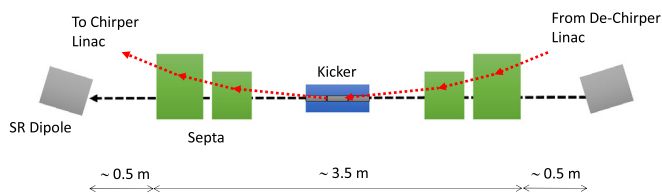
FIG. 9.   Top-view (not to scale) of a fast stripline kicker system in between septum magnets, for on axis swap-out injection into the SRLS (beam travels from right to left), and for extraction from the SRLS at successive turns.

That angle is cancelled by the synchronized field of the kickers.

The scheme illustrated in Fig. 1 foresees the total path length in the by-pass equal to half the ring circumference, i.e., 0.88 μs for one loop. Since we assume kicker repetition rates smaller than 1 MHz, two distinct kicker systems are needed, one for beam injection into the by-pass, and one for beam extraction ∼1 μs later. The two kickers shall be installed contiguous.

B. Linac technology

Different kicker repetition rates imply different values of the beam average current through the loop, hence different linac technology. The two scenarios of 0.1 and 1 kHz in Table IV correspond to, respectively, 2.5 and 50 μA average beam current through the accelerators. Such currents can be managed by pulsed NC rf systems. Although C-band rf technology at 1 kHz is not available on the market, some recent initiatives supported by industrial partners [60–62] indicate that this scenario is well within the horizon of present technical capabilities. The peak accelerating gradient of C-band linacs is, in this case, scaled down to ∼12 MV/m, starting from documented 35 MV/m at 0.1 kHz and by keeping the average rf power constant.

Kicker's repetition rates higher than 10 kHz or so imply mA-level average beam current, and in this case SC linacs become mandatory [63–65]. The very high-FEL pulse repetition rate is obtained at the expense of much lower FEL peak power and a total rf peak voltage as high as ∼0.9 GeV.

A dedicated 0.9 GeV linac would in principle allow lasing at 4 nm with, e.g., a 15 mm-period in-vacuum Apple-X undulator and $K = 1.2$. We note, however, that it could not offer any wavelength tuning, if not at the expense of sub-μJ pulse energies at 4 nm, or unpractical undulator gaps of 1–2 mm for longer wavelengths.

Finally, specification of rms stability in beam mean energy ($<0.1\%$), energy chirp ($<1\%$), and bunch duration ($<5\%$) to and from the compression loop, determines a tolerance on the linacs' rf phase jitter which amounts to $<0.05°$ rms over the entire rf range (L-band to X-band), well within reach of present NC and SC systems.

VIII. CONCLUSIONS

The conceptual and technical feasibility of a high-gain short wavelength FEL driven by a diffraction-limited SRLS is demonstrated via analytical and numerical tools, on the basis of established, state-of-the-art, and cost-effective technology. A novel semi-analytical model for beam envelope tracking was developed, which integrates all major ingredients of electron beam and FEL dynamics, so allowing a fast optimization of the SR-HG-FEL complex.

The FEL beamline is served simultaneously to all other ID beamlines of the storage ring, at a tunable FEL pulse

repetition rate in the range ~1–200 kHz, and at construction and operational costs orders of magnitude lower than a brand new linac-driven FEL in the same wavelength range. At the shortest wavelength of 4 nm considered so far, and for kicker and rf repetition rate in the range 0.1–200 kHz, the SASE FEL single pulse energy is predicted to be in the 1–150 μJ range. Peak power is 1–260 MW over an FEL pulse duration of 0.5 ps rms. The total average FEL power emitted by a bunch train ranges from 0.1 to 10 W in CW mode. In spite of the lower FEL efficiency at very high-repetition rates, the FEL signal is still four orders of magnitude higher than the beam incoherent emission at 100 W level.

In conclusion, the hybrid light source emerges as a new paradigm for the operation of diffraction-limited SRLS, by expanding their capabilities to carry out pump-probe, high-photon flux and timing experiments, where the FEL pulses are naturally synchronized to incoherent emission from storage ring IDs. Its performance can bridge the gap between SRLS and current linac-driven FELs, satisfying the scientific need of time-resolved fine spectroscopic analysis of matter (photoelectric effect and photon scattering) in the linear response regime, as well as inelastic scattering experiments.

The advantages of upgrading an existing SRLS to such hybrid light source has to be traded off with the constraint of fixed electron beam energy, which limits the FEL spectral range compared to facilities driven by a dedicated but far more energetic linac. Nevertheless, the scheme is compatible with modifications of the undulator line devoted, for example, to improved longitudinal coherence (seeding) and multicolor pulses via split undulators, though at reduced pulse energies. Moreover, it can be conceived as a high-repetition rate seeding laser in EUV for a cascade longitudinally coherent FEL into soft and hard x-rays. A detailed evaluation of all these options is, however, not in the scope of this article.

We finally recall that the proposed scheme complements recent proposals of incoherent emission from very short bunches in a SRLS [66,67], as well as a variety of schemes for CHG [20–23,31] as for coherence, peak, and average power.

ACKNOWLEDGMENTS

---

[1] C. Pellegrini, The physics of x-ray free-electron lasers, Rev. Mod. Phys. **88**, 49 (2016).

[2] E. A. Seddon *et al.*, Short-wavelength free-electron laser sources and science: A review, Rep. Prog. Phys. **80**, 115901 (2017).

[3] R. Schonlein, T. Elsaesser, K. Holldack, Z. Huang, H. Kapteyn, M. Murnane, and M. Woerner, Recent advances in ultrafast X-ray sources, Phil. Trans. R. Soc. A **377**, 20180384 (2019).

[4] L.-H. Yu and T. Shaftan, Nat. Photonics **13**, 513 (2019).

[5] S. Di Mitri and M. Cornacchia, Phys. Rep. **539**, 1 (2014).

[6] J. B. Murphy and C. Pellegrini, Nucl. Instrum. Methods Phys. Res., Sect. A **237**, 159 (1985).

[7] K.-J. Kim, J. J. Bisognano, A. A. Garren, K. Halbach, and J. M. Peterson, Nucl. Instrum. Methods Phys. Res., Sect. A **239**, 54 (1985).

[8] K.-J. Kim, J. Bisognano, S. Chattopadhyay, M. Cornacchia, A. Garren, K. Halbach, A. Jackson, H. Lancaster, C. Pellegrini, J. Peterson, G. Vignola, and M. Zisman, IEEE Trans. Nucl. Sci. NS-32, **5**, 3377 (1985).

[9] J. Bisognano, S. Chattopadhyay, M. Cornacchia, A. Garren, K. Halbach, A. Jackson, K.-J. Kim, H. Lancaster, C. Pellegrini, J. Peterson, G. Vignola, and M. Zisman, Part. Accel. **18**, 223 (1986).

[10] M. Cornacchia, J. Bisognano, S. Chattopadhyay, A. Garren, K. Halbach, A. Jackson, K.-J. Kim, H. Lancaster, C. Pellegrini, J. Peterson, G. Vignola, and M. Zisman, Nucl. Instrum. Methods Phys. Res., Sect. A **250**, 57 (1986).

[11] H.-D. Nuhn, R. Tatchyn, H. Winick, A. S. Fisher, and J. Gallardo, Short wavelength FELs on large storage rings, Nucl. Instrum. Methods Phys. Res., Sect. A **319**, 89 (1992).

[12] K. M. Fung, S. Y. Lee, and K. Y. Ng, Feasibility study of storage ring based high gain FEL, in *Proceedings of the 2001 Particle Accelerator Conference, Chicago, IL* (IEEE, Piscataway, NJ, 2001), p. 2730.

[13] G. Dattoli, E. Di Palma, A. Petralia, and J. V. Rau, SASE FEL storage ring, IEEE J. Quantum Electron. **48**, 1259 (2012).

[14] R. R. Lindberg, Y. Cai, K.-J.- Kim, and Z. Huang, Trans-verse gradient undulators for a storage ring-based x-ray FEL oscillator, in *Proceedings of the 35th International Free-Electron Laser Conference, New York, NY, USA*, edited by C. Scholl and V. Schaa (JACoW, Geneva, Switzerland, 2013), THOBNO02, ISBN 978-3-95450-126-7.

[15] Y. Cai, Y. Ding, R. Hettel, Z. Huang, L. Wang, and L. Xiao, Synchrotron Radiat. News **26**, 39 (2013).

[16] Y. Ding, P. Baxevanis, Y. Cai, Z. Huang, and R. Ruth, in *Proceedings of the Fourth International Particle Accelerator Conference, Shanghai, China*, edited by Z. Dai, C. Petit-Jean-Genaz, V. Schaa, and C. Zhang (JACoW, Geneva, 2013), WEPWA075, ISBN 978-3-95450-122-9.

[17] I. Agapov, Nucl. Instrum. Methods Phys. Res., Sect. A **793**, 35 (2015).

[18] S. Di Mitri and M. Cornacchia, New J. Phys. **17**, 113006 (2015).

[19] Z. Huang, K. Bane, Y. Cai, A. Chao, R. Hettel, and C. Pellegrini, Nucl. Instrum. Methods Phys. Res., Sect. A **593**, 120 (2008).

[20] C. Evain, A. Loulergue, A. Nadji, J. M. Filhol, M. E. Couprie, and A. A. Zholents, Soft x-ray femtosecond coherent undulator radiation in a storage ring, New J. Phys. **14**, 023003 (2012).

[21] C. Feng and Z. Zhao, A storage ring-based free-electron laser for generating ultrashort coherent EUV and x-ray radiation, Sci. Rep. **7,** 4724 (2017).

[22] J.-G. Hwang, G. Schiwietz, M. Abo-Bakr, T. Atkinson, M. Ries, P. Goslawski, G. Klemz, R. Müller, A. Schälicke, and A. Jankowiak, Generation of intense and coherent sub-femtoseocnd x-ray pulses in electron storage rings, Sci. Rep. **10,** 10093 (2020).

[23] C. Li, C. Feng, and B. Jiang, Extremely bright coherent synchrotorn radiation production in a diffraction-limited storage ring using angular dispersion-induced microbunching scheme, Phys. Rev. Accel. Beams **23,** 110701 (2020).

[24] A. M. Kondratenko and E. L. Saldin, Part. Accel. **10,** 207 (1980), https://inspirehep.net/files/872da099a0e9c171a-4dca19256f7ca0e.

[25] R. Bonifacio, C. Pellegrini, and L. Narducci, Opt. Commun. **50,** 373 (1984).

[26] L. Serafini et al., MariX, an advanced MHz-class repetition rate x-ray source for linear regime time-resolved spectroscopy and photon scattering, Nucl. Instrum. Methods Phys. Res., Sect. A **930,** 167 (2019).

[27] T. Smith, J. M. J. Madey, L. R. Elias, and D. A. G. Deacon, J. Appl. Phys. **50,** 4580 (1979).

[28] N. Kroll, P. Morton, M. Rosenbluth, J. Eckstein, and J. M. J. Madey, IEEE J. Quantum Electron. **17,** 1496 (1981).

[29] L. Emery and M. Borland, Possible long-term improvements to the advanced photon source, Proceedings of the 20th Particle Accelerator Conference, PAC-2003, Portland, OR, 2003 (IEEE, New York, 2003), TOPA014, p. 256.

[30] D. F. Ratner and A. W. Chao, Steady-State Microbunching in a Storage Ring for Generating Coherent Radiation, Phys. Rev. Lett. **105,** 154801 (2010).

[31] X. Deng, A. Chao, J. Feikes, A. Hoehl, W. Huang, R. Klein, A. Kruschinski, J. Li, A. Matveenko, Y. Petenev, M. Ries, C. Tang, and L. Yan, Experimental demonstration of the mechanism of steady-state microbunching, Nature (London) **590,** 576 (2021).

[32] A. Renieri, IEEE Trans. Nucl. Sci. **26,** 3827 (1979).

[33] Y. K. Wu, J. Yan, H. Hao, J. Y. Li, S. F. Mikhailov, V. G. Popov, N. A. Vinokurov, S. Huang, and J. Wu, Widely Tunable Two-Color Free-Electron Laser on a Storage Ring, Phys. Rev. Lett. **115,** 184801 (2015).

[34] M. Borland, Ultra-low emittance light sources, in Synchrotron Radiation News, edited by R. Frahm, M. C. Martin, and M. Suzuki (Taylor and Francis, Philadelphia, PA, 2014), Vol. 27, p. 2.

[35] S. Leemann, Interplay of Touschek scattering, intrabeam scattering, and rf cavities in ultralow-emittance storage rings, Phys. Rev. ST Accel. Beams **17,** 050705 (2014).

[36] K.-J. Kim, Nucl. Instrum. Methods Phys. Res., Sect. A **246,** 71 (1986).

[37] D. R. Douglas, Thomas Jefferson National Accelerator Facility Technical Report No. JLAB-TN-98-012, 1998.

[38] S. Di Mitri, M. Cornacchia, and S. Spampinati, Phys. Rev. Lett. **110,** 014801 (2013).

[39] Ya. S. Derbenev, J. Rossbach, E. L. Saldin, and V. D. Shiltsev, DESY, Hamburg, Germany, Report No. TE-SLA-FEL 95-05, 1995.

[40] E. L. Saldin, E. A. Schneidmiller, and M. V. Yurkov, Nucl. Instrum. Methods Phys. Res., Sect. A **398,** 373 (1997).

[41] S. Di Mitri and M. Cornacchia, Europhys. Lett. **109,** 62002 (2015).

[42] S. Di Mitri, Nucl. Instrum. Methods Phys. Res., Sect. A **806,** 184 (2016).

[43] M. Borland, APS Tech Note No. LS-207, 2000.

[44] A. Brynes et al., Beyond the limits of 1D coherent synchrotron radiation, New J. Phys. **20,** 073035 (2018).

[45] S. Di Mitri, C. Venier, R. Vescovo, and L. Sturari, Wake-field benchmarking at a single-pass high brightness electron linac, Phys. Rev. Accel. Beams **22,** 014401 (2019).

[46] P. Baxevanis, Y. Ding, Z. Huang, and R. Ruth, Phys. Rev. ST Accel. Beams **17,** 020701 (2014).

[47] G. Dattoli and P. L. Ottaviani. Semi-analytical models of free electron laser saturation, Opt. Commun. **204,** 283 (2002).

[48] S. Reiche, GENESIS1.3: A fully 3D time-dependent FEL simulation code, Nucl. Instrum. Methods Phys. Res., Sect. A **429,** 243 (1999).

[49] M. Calvi, C. Camenzuli, E. Prata, and T. Schmidt, Transverse gradient in Apple-type undulators, J. Synchrotron Radiat. **24,** 600 (2017).

[50] T. Schmidt and M. Calvi, APPLE X undulator for the Swiss FEL soft X-ray beamline athos, Synchrotron Radiat. News **31,** 35 (2018).

[51] E. Wallén et al., Status of the LCLS-II undulators, AIP Conf. Proc. 1741, 020025 (2016).

[52] J. Lee, G. Jang, J. Kim, B. Oh, D.-E. Kim, S. Lee, J.-H. Kim, J. Ko, C. Min, and S. Shin, Demonstration of a ring-FEL as an EUV lithography tool, J. Synchrotron Radiat. **27,** 864 (2020).

[53] Z. Huang, Y. Ding, and C. B. Schroeder, Phys. Rev. Lett. **109,** 204801 (2012).

[54] D. Alesini, S. Guiducci, F. Marcellini, and P. Raimondi, Phys. Rev. ST Accel. Beams **13,** 111002 (2010).

[55] T. Naito, H. Hayano, M. Kuriki, N. Terunuma, and J. Urakawa, Development of a 3 ns rise and fall time strip-line kicker for the International Linear Collider, Nucl. Instrum. Methods Phys. Res., Sect. A **571,** 599 (2007).

[56] T. Naito, S. Araki, H. Hayano, K. Kubo, S. Kuroda, N. Terunuma, T. Okugi, and J. Urakawa, Multibunch beam extraction using the strip-line kicker at the KEK Accelerator Test Facility, Phys. Rev. ST Accel. Beams **14,** 051002 (2011).

[57] P. Emma et al., in Proceedings of FEL14, Basel, Switzerland, edited by J. Chrin, S. Reiche, and V. Schaa (JACoW, Geneva, Switzerland, 2015), THP025, ISBN 978-3-95450-133-5.

[58] S. Kwiatkowski et al., "Camshaft" bunch kicker design for the ALS storage ring, Proc. of Europ. Part. Accel. Conf., THPLS114, Edinburgh, Scotland, UK (2006).

[59] C. Sun, G. Portmann, M. Hertlein, J. Kirz, and D. S. Robin, Phys. Rev. Lett. **109,** 264801 (2012).

[60] G. D'Auria et al., Status of the compact light design study, in Proceedings of the 39th International Free-Electron laser Conference Hamburg, Germany, edited by W. Decking, H. Sinn, G. Geloni, S. Schreiber, V. Schaa, and M. Marx (JACoW, Geneva, Switzerland, 2019), THP078, ISBN 978-3-95450-210-3.

[61] S. Di Mitri *et al.*, Scaling of beam collective effects with bunch charge in the compact light free-electron laser, Photonics **7**, 125 (2020).

[62] M. Volpi *et al.* High power and high repetition rate x-band power source using multiple klystrons, in *Proceedings of the 9th International Particle Accelerator Conference, Vancouver, Canada* (JACoW, Geneva, 2018), THPMK104 4552.

[63] S. V. Benson, D. R. Douglas, P. Evtushenko, F. E. Hannon, C. Hernandez-Garcia, J. M. Klopf, R. A. Legg, G. R. Neil, M. D. Shinn, C. D. Tennant *et al.*, J. Mod. Opt. **58**,16 1438 (2011).

[64] Z. Liu and A. Nassiri, Phys. Rev. ST Accel. Beams **13**, 012001 (2010).

[65] W. Singer *et al.*, Production of superconducting 1.3-GHz cavities for the European X-ray Free Electron Laser, Phys. Rev. ST Accel. Beams **19**, 092001 (2016).

[66] H. Owen, P. H. Williams, and S. Stevenson, Nonequilibrium Electron Rings for Synchrotron Radiation Production, Phys. Rev. Lett. **110**, 154801 (2013).

[67] X. Huang, T. Rabedeau, and J. Safranek, Generation of picosecond electron bunches in storage rings, J. Synchrotron Radiat. **21**, 961 (2014).